Available online at www.sciencedirect.com
ScienceDirect
Journal of the European Ceramic Society 29 (2009) 223–236
www.elsevier.com/locate/jeurceramsoc

AlON: A brief history of its emergence and evolution

James W. McCauley [a,*], Parimal Patel [a], Mingwei Chen [b,c], Gary Gilde [a], Elmar Strassburger [d], Bhasker Paliwal [c], K.T. Ramesh [c], Dattatraya P. Dandekar [a]

[a] *U.S. Army Research Laboratory, APG, Maryland, USA*
[b] *Tohoku University, Japan*
[c] *The Johns Hopkins University, USA*
[d] *Fraunhofer-Institut für Kurzzeitdynamik, Ernst-Mach-Institut (EMI), Efringen-Kirchen, Germany*

Available online 20 June 2008

Abstract

In the early 1970s in Japan, the United States and France it was found that additions of nitrogen into aluminum oxide resulted in new spinel-like phases. At about the same time there was much increased interest in oxynitrides, stimulated by Professor K. Jack in the UK and Y. Oyama in Japan. Following these activities a major research program in this area was initiated at the Army Materials and Mechanics Research Center in Watertown, Massachusetts in 1974. These efforts resulted in the first complete Al_2O_3–AlN phase equilibrium diagram and a process to reactively sinter to nearly full density, translucent aluminum oxynitride spinel ceramic, which was named AlON. Subsequently, the Raytheon Company further developed AlON into a highly transparent material (ALON™) with many applications including transparent armor and EM domes and windows, among others—the technology was recently transferred to the Surmet Corporation. This paper will review the early history, phase equilibrium, crystal chemistry, and properties of this material, along with more recent work in our laboratory on transient liquid phase sintering and new data on lattice parameter measurements. In addition, recent results of collaborative work on AlON's dynamic mechanical properties using plate impact, Kolsky bar and edge-on impact (EoI) experimental techniques, including preliminary modeling at the microstructural scale of AlON in the EoI test, will be presented.
Published by Elsevier Ltd.

Keywords: AlON; History; Phase equilibrium; Processing; Properties

1. Early history

In 1959 Yamaguchi and Yanagida[1] reported on the possibility of a spinel-type phase in the Al_2O_3–AlN system. Over the next several years[2–6] other research confirmed that a spinel phase did exist in this system. In 1972 two papers came out within a short period of time of each other[7,8] dealing with reactions and phases in the Si_3N_4–Al_2O_3–AlN system that catalyzed a period of extensive work in this system. A key aspect of this system was the phase equilibrium in the Al_2O_3–AlN pseudo-binary system, especially as it had to do with the formation of SiAlONs—apparent solid solutions of Al and O in the Si_3N_4 structure. Ken Jack, University of Newcastle upon Tyne, spearheaded an enormous amount of research in this field world wide. One of the early questions concerned the location of the join in the ternary system where the SiAlON solid solution occurred: Si_3N_4–Al_2O_3 or Si_3N_4–Al_3O_3N (apparent ideal spinel composition). As this activity commenced in early 1973,[9] it became fairly clear that there were some apparent discrepancies in the existing Al_2O_3–AlN phase diagram. At this same time there was significant interest in new transparent armor materials and thermal-mechanically stable electromagnetic windows and domes. These two drivers merged focusing attention on refining the phase equilibrium diagram and attempting to produce fully dense materials based on the assumed cubic Al–O–N spinel phase in this system.[10,11] Following this preliminary work, a model was developed[12] which then guided the phase equilibrium and processing efforts[13] toward the fabrication of the first close to transparent AlON material (Fig. 1) and the first AlON patent.[14] Collaborations with the Raytheon Company commenced in 1977 with Dr. Rick Gentilman, Ed Maguire and Tom Hartnett.[15] Several more Raytheon patents ensued.[16] McCauley and Corbin continued this work completing the full Al_2O_3–AlN phase equilibrium diagram, including the addition of the various AlN polytypoid phases[17,18] and the first comprehensive review in

* Corresponding author.
E-mail address: mccauley@arl.army.mil (J.W. McCauley).

0955-2219/$ – see front matter. Published by Elsevier Ltd.
doi:10.1016/j.jeurceramsoc.2008.03.046

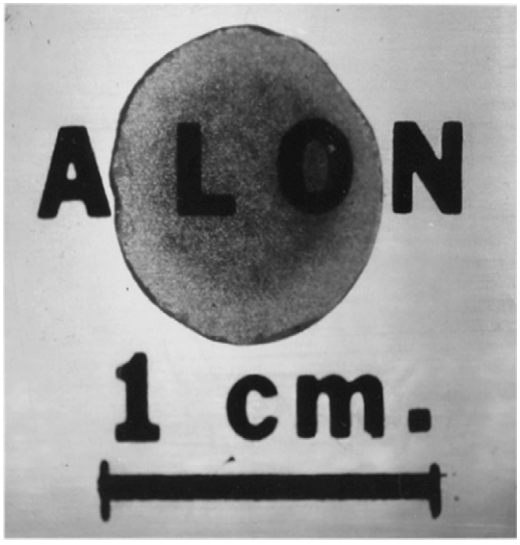

Fig. 1. First translucent AlON disc produced by McCauley and Corbin[13]—circa 1976.

1989.[19] More recently, three additional reviews have been published.[20,21,22]

2. Fundamental studies

2.1. Phase equilibrium

In classic work, Lejus,[4] published the first phase diagram of the Al_2O_3–AlN system in 1964 which is illustrated in Fig. 2a, indicating a γ-phase centered at about 75 mol% Al_2O_3. Gauckler and Petzow followed this with a diagram (Fig. 2b) that included selected AlN-based polytypoids.[23] McCauley and Corbin[13] published a new diagram (Fig. 3a) in the region of the AlON solid solubility region, showing the composition centered at about 35.7 mol% AlN. This was followed in 1983[17] and 1988[18] by a more complete phase equilibrium diagram (Fig. 3b) for the pseudo-binary Al_2O_3–AlN composition join, determined experimentally. The solid line at about 1700 °C represents the temperature at which equilibrium could not be reached conveniently. It is important to point out some of the key aspects of this diagram: since AlN sublimes at these conditions, whereas alumina melts, the diagram contains solid/vapor, liquid/vapor and liquid/solid equilibrium; three liquid/solid eutectics; one vapor/solid eutectic; several polytypoid phases are also present—there are others that have been identified, but it is not clear where their stability regions are located. (Refer to references[17,18,20] for more details on the polytypoid materials.) Fukuyama et al.[24] in using plasma arc melting to produce AlON powder, seems to have confirmed the vapor/liquid relationships in the extreme temperature region. A more recent experimental phase diagram has been determined by Willems et al.[25] (Fig. 3c). Our original work[13] suggested that AlON melts incongruently, however, in subsequent experiments and analysis it was concluded that for the conditions of these experiments (i.e. about one atmosphere of flowing nitrogen) AlON did melt congruently, but this is probably a function of the total overpressure

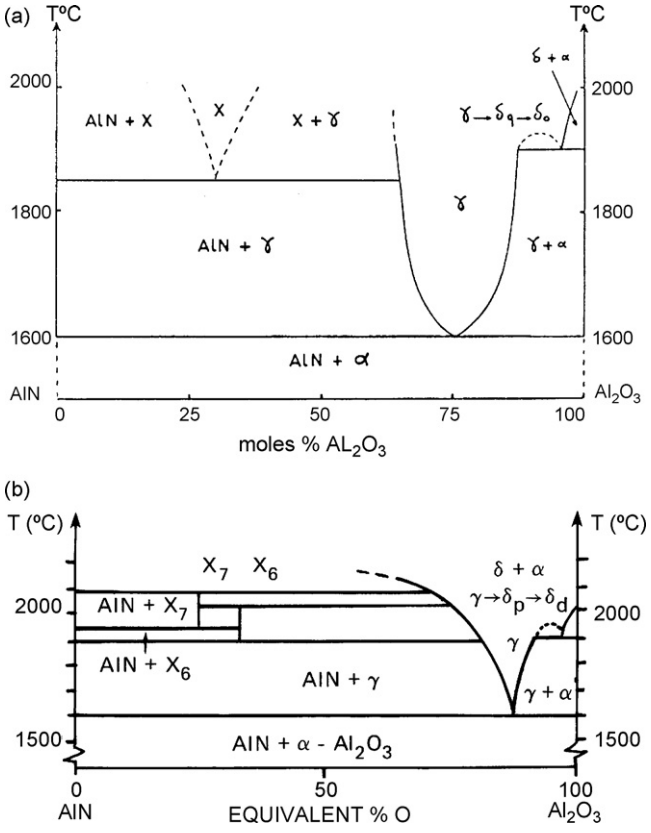

Fig. 2. (a) First phase diagram of the Al_2O_3–AlN system, Lejus;[4] (b) Gauckler and Petzow, 1977.[23]

and the pressure media (gas composition). For more information on these complex phase equilibrium issues see Zernike.[26]

Almost in parallel with the experimental determination of the phase equilibrium diagram, many workers have attempted to calculate the AlON stability region and the full Al_2O_3–AlN system using available thermodynamic data and experimental identification of the various phases in the system. Kaufman[27] calculated the first diagram of this system which is illustrated in Fig. 4a. Dumitrescu and Sundman[28] calculated the first comprehensive diagram of the pseudo-binary system. Fig. 4b illustrates this diagram together with available experimental data. Other calculated diagrams have also been produced.[29,30] Tabary and Savant[30] also calculated the liquid/vapor equilibrium (Fig. 4c) which is in general agreement with the proposed diagram of McCauley et al.[18] Additional works determining the thermodynamic properties of AlON and related materials have been carried out.[31–35]

2.2. Processing summary

Over the years several different processing routes have been used to produce fully dense, transparent polycrystalline AlON ceramics. Initial work by McCauley and Corbin[13] used reaction sintering of Al_2O_3–AlN mixtures. The reaction sintering technique has also been used by others as well.[36–38] However, other pressureless sintering, hot pressing and hot isostatic pressing (HIP) techniques have been used starting with AlON powders to

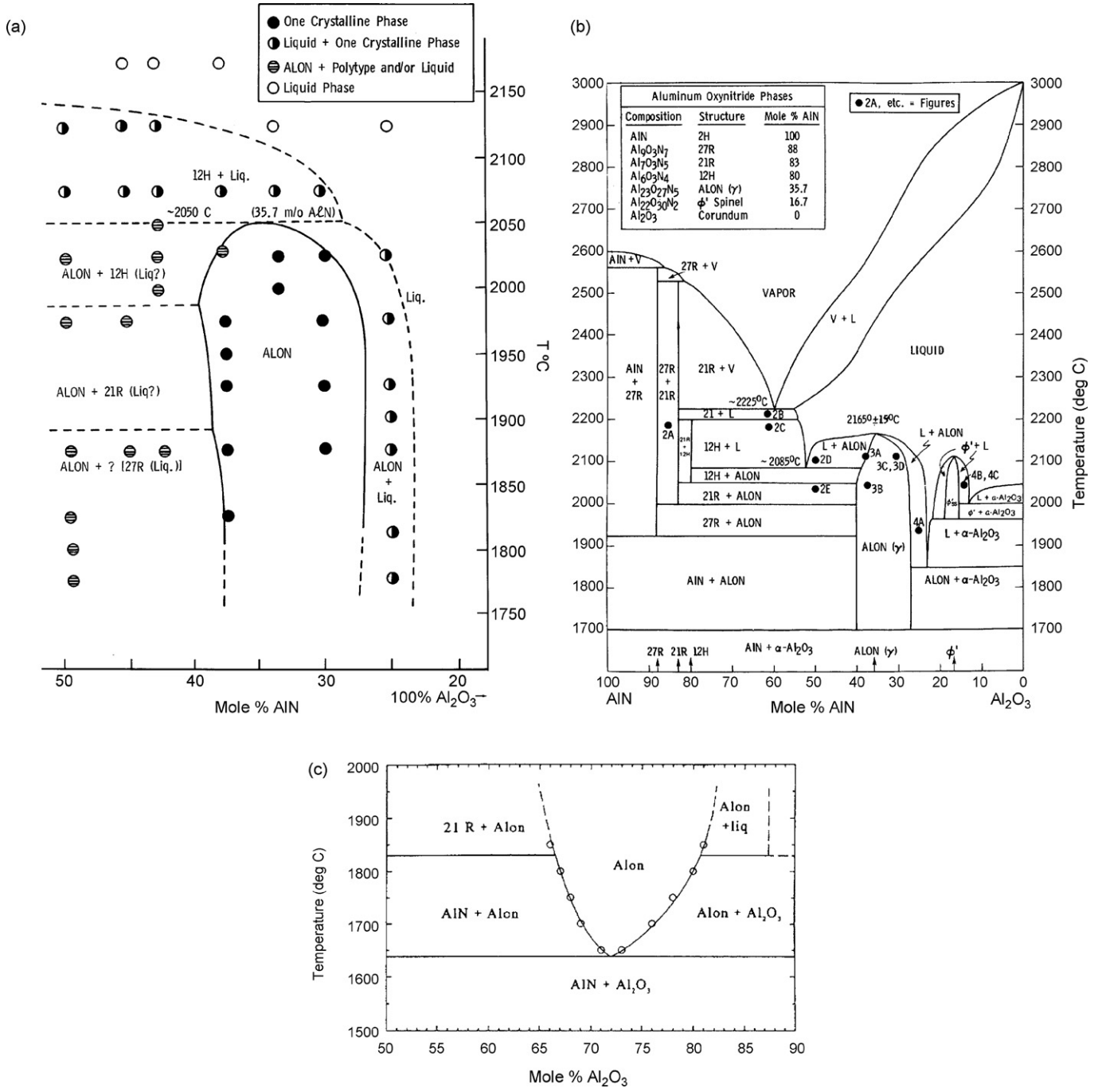

Fig. 3. (a) AlON detail in the Al_2O_3–AlN system;[13] (b) proposed experimental phase equilibrium diagram for the pseudo-binary Al_2O_3–AlN composition join at one atmosphere of flowing nitrogen;[17] taken from Ref. 17, figure 1, p. 112, with kind permission of Springer Science and Business Media (c) experimental diagram from Willems et al.[25]

produce pore free, fully dense AlON ceramics.[39–41] AlON powders can be synthesized by simple reaction of Al_2O_3 and AlN, carbothermal reduction of Al_2O_3,[42] plasma arc synthesis[24,43] and self-propagating high-temperature synthesis (SHS).[44]

In a more comprehensive study,[45,46] the properties of materials in the Al_2O_3–AlN system by both reactive hot-pressing and reaction-sintering was studied, referring to these materials as ALUMINALON. Significant variations in hardness, flexure strength and fracture toughness were observed. The friction, wear resistance and other mechanical properties of the Al_2O_3–AlON family of materials has also been systematically studied.[47,48] In addition, insulation and refractory applications have been reported.[49,50]

2.3. Crystal chemistry

Fig. 5 summarizes selected phase equilibrium, bonding and atomic structure changes in this system. The bonding changes from primarily ionic in α-Al_2O_3 to covalent in AlN. The electronegativities of Al = 1.5, O = 3.5 and N = 3.0 result in predicted

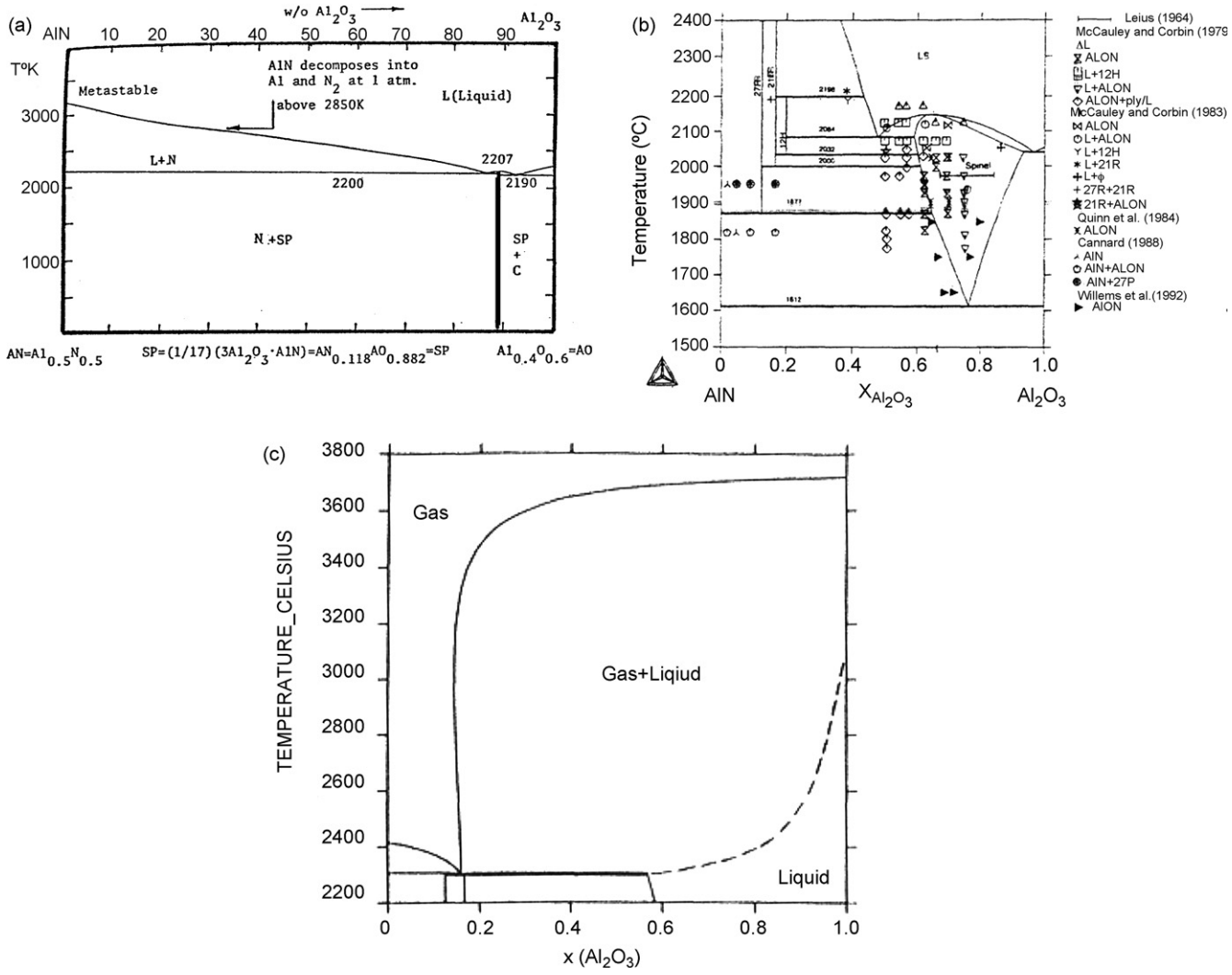

Fig. 4. (a) First calculated phase diagram from Kaufman[27] (b) Dumitrescu and Sundman calculated phase diagram[28] with several experimental data points, (c) calculated gas (vapor)/liquid equilibrium from Tabary and Savant.[30]

ionic character of α-Al_2O_3 at 63%, AlN at 43% and AlON at about 56%. Structurally, the substitution of oxygen into AlN or nitrogen into Al_2O_3 de-stabilizes the parent structures with the resulting formation of modulated structures. Conceptually,

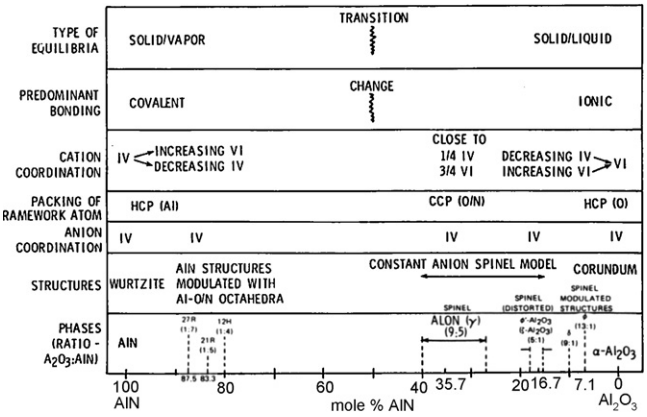

Fig. 5. Crystal chemistry relationships in the Al_2O_3–AlN system. (McCauley and Corbin).[17] taken from Ref. 17, p. 117, with kind permission of Springer Science and Business Media.

nitrogen substitution into Al_2O_3 causes a local charge imbalance on the substituted nitrogen. This can be reduced by a shift in anion coordination around Al from 6 to 4, driving the α-Al_2O_3 based phase toward a spinel ($MgAl_2O_4$) type structure, where the cations are distributed between octahedral and tetrahedral coordination. This has been confirmed by crystal structure analysis of AlON,[51,52] and more recently by *ab initio* calculations,[53] confirming the predictive model.[12] Basically, in the AlON spinel unit cell, there are 8 Al cations in tetrahedral sites, and 15 Al and one vacancy in the 16 octahedral sites. Fig. 6 shows the magic angle spinning nuclear magnetic resonance of ^{27}Al spectra in 37.5 and 30 mol% AlN Raytheon ALON™ using a Bruker AM-400 (9.4 T) at <5 kHz.[54] The peaks clearly show that Al is in both tetrahedral and octahedral coordination. Superscripts are coordination numbers.

$$Al_8^{IV}\,Al_{15}^{VI}\,\square^{VI}\,O_{27}\,N_5$$

□ = a cation vacancy

The constant anion model, which assumes a constant number (32) of anions in a spinel unit cell, has successfully been used

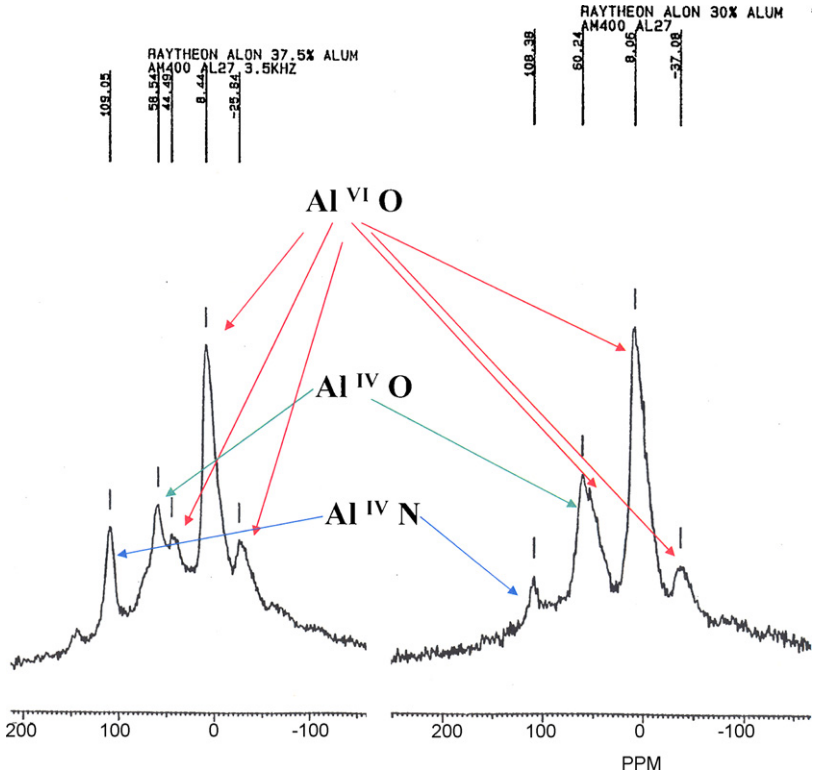

Fig. 6. Magic angle spinning nuclear magnetic resonance of ^{27}Al spectra in 37.5 and 30 mol% AlN Raytheon ALON™. (Leffler, Burum, Appel, Carreiro, and McCauley, 1985, unpublished).

to describe and account for the unconventional (seemingly non-stoichiometric) composition of both the AlON (N = 5) and the ϕ′ (N = 2) phases.[20] The model assumes the following formula:

$$\mathbf{Al_{(64+x)/3}\,\square_{(8-x)/3}\,O_{(32-x)}N_x}.$$

The "normal" spinel composition (N = 8) does not seem to be a stable phase, whereas AlON (N = 5) and ϕ′ (N = 2) are seemingly stable, stoichiometric phases, verified by many investigators.

2.4. Lattice parameter/composition relationships

It would be very useful to be able to determine the exact AlON composition from refined lattice parameters, however, there have been some small, but systematic differences between the various measurements of other investigators[13,25,56] that are nicely summarized by Schwarz[55] in Fig. 7. In this figure he extrapolates the SiAlON and AlON data to the hypothetical "ideal" AlON composition of Al_3O_3N—which has not been observed experimentally yet.

The AlON lattice parameter data summarized on this figure has been obtained on materials that have been processed differently. For example, Willems[25] investigated the phase relations for this system for temperatures below 1850 °C. In earlier[13] works, it was noted that in one atmosphere of flowing nitrogen, the weight loss changed from about 3% below about 1975 °C to 9% above this temperature, strongly suggesting a significant change in composition from the starting material. In addition, the experimental evidence in that same study suggested that there is a processing temperature window with a lower temperature above which the material is at equilibrium and the nitrogen is homogeneously distributed and another higher temperature at which the AlON becomes unstable with more excessive weight loss from vaporization. A recent investigation[57] also indicated the requirement for elevated processing gas pressure to stabilize the system above 1950 °C. Fig. 8 is a plot of historical data of lattice parameter versus initial batched composition, a convention we assume was used by all the previous investigators of AlON. The data reported earlier[13] were determined from AlON samples processed at 1975 °C. The data can be separated into two distinct groups. Though the slopes for the sets are uniform, there is disparity on the lattice parameter of the processed parts.

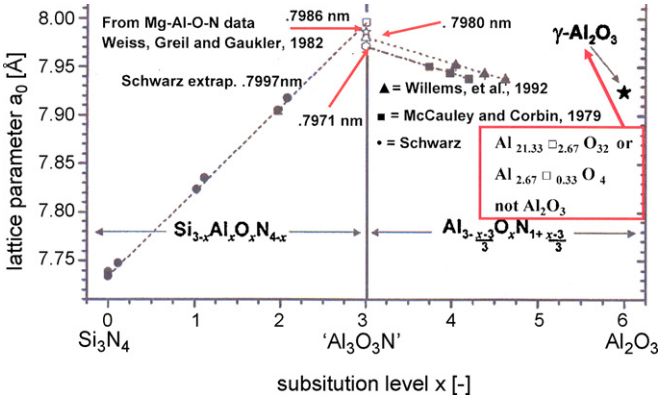

Fig. 7. Lattice parameters of a variety of Si–Al–O–N-based materials. Modified from Marcus Rolf Schwarz.[55]

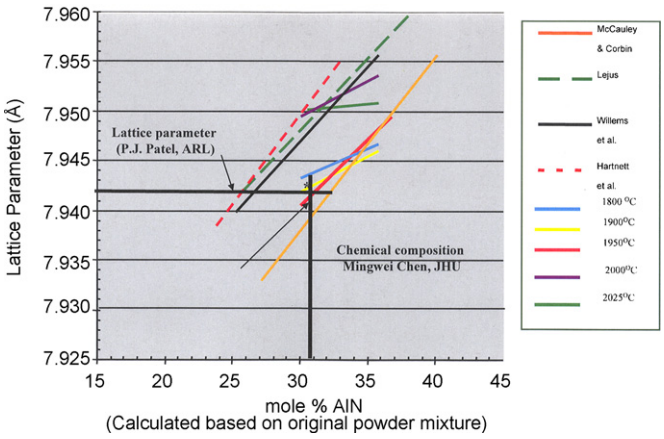

Fig. 8. AlON composition vs. lattice parameter data from several authors, including new ARL data at various temperatures, and a new data point for a Surmet ALON^{TM} sample.

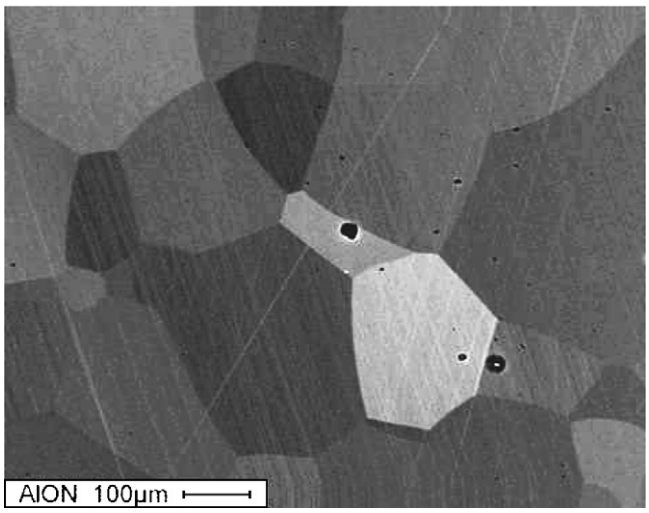

Fig. 9. Backscattered electron image of AlON used in this study.

The straight lines in Fig. 8 all have an important assumption that the composition of the final processed part is identical to the batched composition. This appears to be incorrect as determined by Patel[57] who measured the lattice parameter as a function of process temperature for the entire AlON homogeneity field. A significant shift in lattice parameter signifying a loss of oxygen was shown. Furthermore, a weight loss was measured for all temperatures greater than 1800 °C with weight loss of 5% or greater for materials processed greater than 1950 °C. This data signifies that the processed parts cannot have the same composition as the original batched composition, unless the vaporization was congruent. To date, it does not appear that a quantitative analysis of all three elements has been determined for a processed material.

Table 1
Quantitative EDS measurements of AlON

Measurement (at.%)	Nitrogen (at.%)	Oxygen (at.%)	Aluminum (at.%)	N_N/N_O
#1	7.64	51.62	40.74	0.148
#2	7.71	51.63	40.66	0.149
#3	7.82	51.53	40.65	0.152

In order to resolve the uncertainty in the relation of the AlON lattice parameter to composition, a sample of ALON^{TM} procured from the Raytheon Corporation, now sold by Surmet Corporation, was used for this study. X-ray diffraction analysis was performed on the samples to verify that AlON was

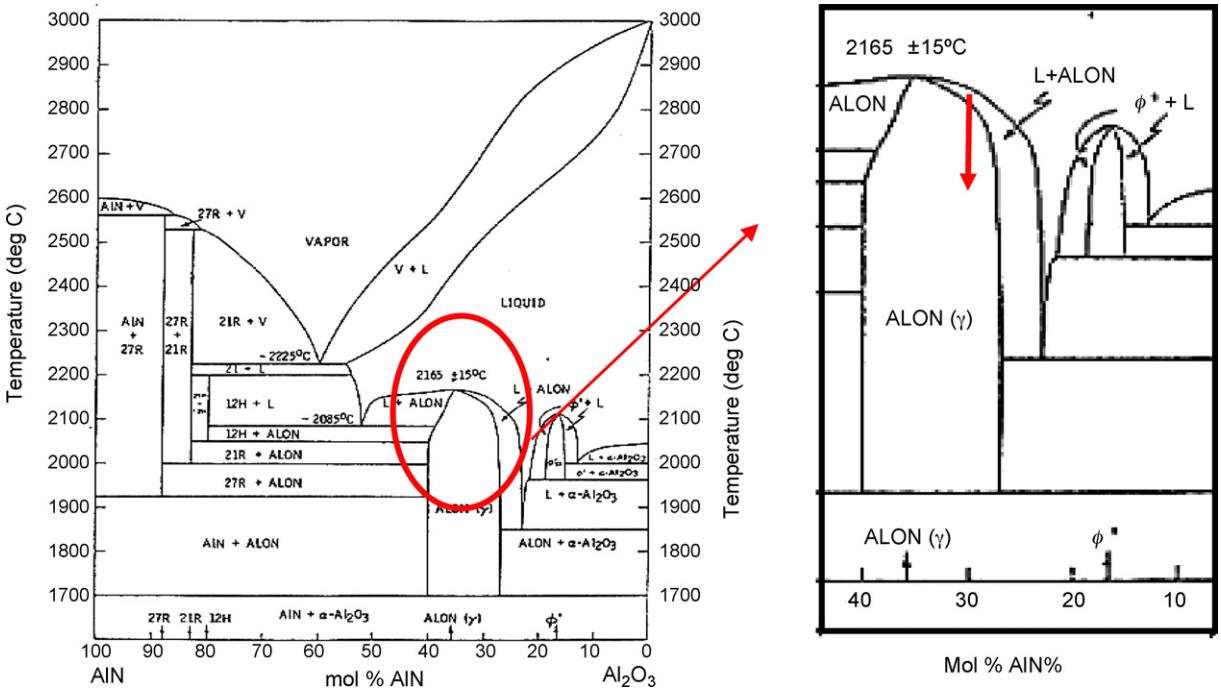

Fig. 10. Phase diagrams illustrating transient liquid phase sintering.

the only phase present. The lattice parameter was calculated by a least squares extrapolation against a standard function using the diffraction peaks with high two-theta angles. The composition was measured using energy dispersive spectroscopy (EDS). Fig. 9 illustrates the microstructure of the AlON material. Table 1 lists the EDS composition results.

The lattice parameter was determined to be 0.7942 nm with an average EDS composition as follows: 40.68% Al, 51.59% O, 7.72% N. This equates to 30.98 mol% AlN and 69.01 mol% Al_2O_3. These data are plotted in Fig. 8, corresponding more closely with the earlier results.[13] Some tentative conclusions can be drawn from these experiments:

- ~1800–1950 °C: lattice parameter increases linearly with nitrogen content; differing slopes.
- ~1950–1975 °C: lattice parameter begins to vary non-linearly.
- ~2000 °C: lattice parameter no longer increases linearly with nitrogen content.
- For fixed initial composition, the lattice parameter is greater at 2000 °C compared to the value at 1800 °C.
- Earlier data[13] are shifted over to nitrogen rich side when compared to other investigations.
- These new results seem to support the earlier data[13] for process temperatures less than about 2000 °C:
  (1) composition changes (lattice parameter) with process temperatures >1975 °C;
  (2) incorrect to use original batch composition as point of comparison;
  (3) need actual composition of processed AlON to accurately compare data using lattice parameter.

- Below about 1975 °C competing reactions seem to be occurring: nitrogen incorporation into AlON and oxygen loss.
- As temperature is increased, above about 1975 °C:
  (1) Oxygen removal dominates, possibly as Al_2O.
  (2) Suggest importance of vapor phase and processing over pressure.

In the following section these issues will be addressed in more detail.

3. Transient liquid phase sintering and effect of pressure

As discussed previously, AlON has been produced by several techniques such as sintering, reaction sintering, hot-pressing and, in some cases, hot isostatic pressing (HIP). The removal of porosity and reduction of secondary phases is critical for transparency. Patel[57] has recently investigated transient liquid phase sintering of AlON as a new, viable processing technique to fabricate fully dense, transparent material. Transient liquid phase sintering introduces a small fraction of liquid that aids in pore elimination and densification. In a single step, the material is shifted from the liquid/solid region into the AlON solid solution region.[58] In the solid solution stability field, the liquid is fully reacted with the solid AlON phase while further densification occurs. Fig. 10 shows a schematic of the transient liquid phase process. Fig. 11 illustrates a typical disc produced by this process.

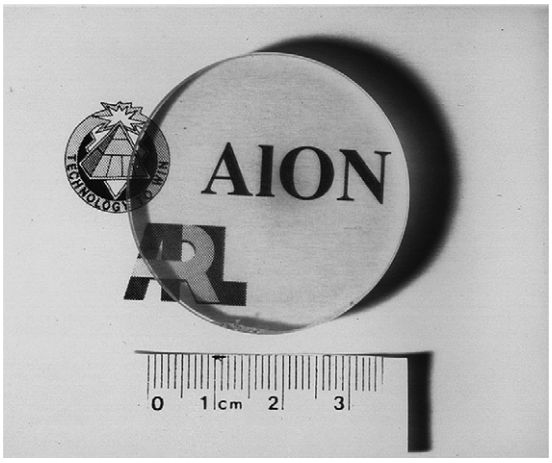

Fig. 11. AlON disc (6 mm thick) densified using transient liquid phase sintering (29.7 psia).

As discussed previously, weight losses increase above ~1950–1975 °C, accompanied by changes in the relative composition as determined by lattice parameter measurements, probably due to the formation of a vapor phase at elevated temperatures, either from liquid or solid. At elevated temperatures, the composition was found to migrate towards layer lattice parameters, and thus, a higher nitrogen content material.[19] Fig. 12 illustrates the surprisingly strong dependence of the AlON lattice parameter on nitrogen pressure at 2000 °C which results in weight loss as the temperature is increased to 2000 °C. A reduced lattice parameter would signify the loss of nitrogen content, or a shift in the composition of the material towards the Al_2O_3 side of the pseudo-binary phase diagram. Increasing nitrogen content is equivalent to reducing oxygen content, and it is the relative change in ratio, which is reflected in the lattice parameter. However, the observation is a net *reduction* in nitrogen content (i.e., more relative oxygen) as nitrogen pressure is increased. One explanation is the suppression of an oxygen rich vapor phase, in the form of Al_2O,[59] as pressure is increased. Nitrogen is believed not to be reactive under these conditions and no significant nitrogen dissolution into AlON occurs. Finally, as can be seen in Fig. 13, it was determined that the lattice parameter of AlON decreased from 0.7960 to 0.7926 nm as the

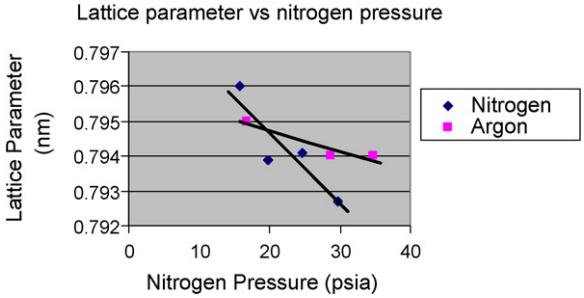

Fig. 12. Lattice parameter vs. nitrogen and argon pressure for 28 mol% AlN heated at 2000 °C for 0.5 h.

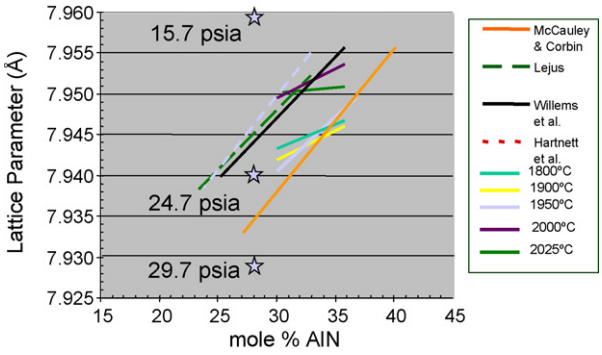

Fig. 13. Lattice parameter vs. mol% AlN at various N_2 pressures at 2000 °C.

over pressure was increased from 0.11 (15.5 psia) to 0.2 MPa (29.5 psia).

In summary:

- Lattice parameter increases with nitrogen content.
- Lattice parameter decreases with increasing oxygen content.
- Increasing nitrogen or argon pressure stabilizes the system suppressing oxygen loss (Al_2O).

4. AlON properties

McCauley[20] has tabulated most of the properties of AlON and the reader is referred to that paper for details. New work concerning the micro-hardness of AlON has been recently published (Fig. 14a)[60] as well as a more comprehensive set of data by Hartnett.[61] Almost all of the property data has been obtained on ALON™ with grain sizes on the order of 150–200 μm, which is illustrated in Fig. 14b. It is not known how the properties would change with grain size, especially at the nano-grain size level (<about 500 nm).

In some of AlON's applications it is subjected to severe impacts at very high rates. A critical factor to further accelerating the optimization of AlON is development of validated predictive performance computer models. This approach is based on the determination and quantification of the various energy absorption mechanisms, including the various deformation modes, damage nucleation and accumulation processes, and the resulting eventual failure at high rates under very high impact stress (shock wave); at the root of this problem is the identification of the fundamental macro and micro (nano) mechanisms of deformation and failure.

It is, therefore, extremely important to determine the dynamic mechanical properties of this material, including the high rate/high stress deformation and damage mechanisms that lead to failure, including the influence of defects and microstructure, including anisotropic elasticity. In addition, AlON can serve as a model material for polycrystalline ceramics and, because of its transparency, real time diagnostic observations can be easily carried out in many mechanical tests.

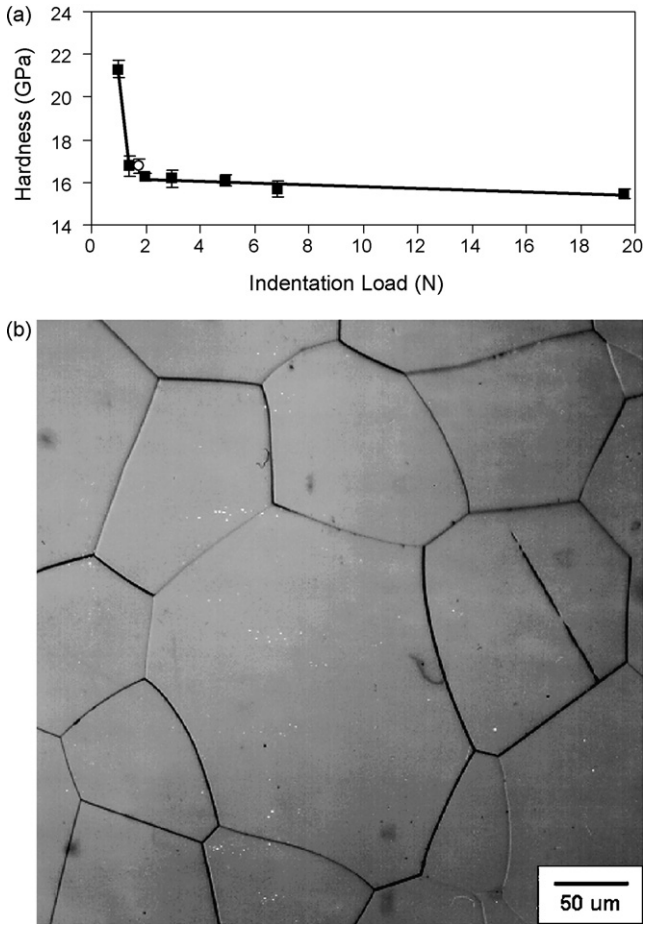

Fig. 14. (a) Hardness-load (Vickers) curve for aluminum oxynitride spinel;[60] (b) SEM photomicrograph of a typical ALON™ material.[60]

4.1. Elastic constants

Table 2 compares the c_{ij} elastic constants obtained by Graham et al.[62] to more recent work using resonant ultrasound spectroscopy (RUS).[63,64] The c_{12} constant still needs to be determined unambiguously from a single crystal to confirm the RUS results.

Table 2
Elastic Constants for AlON

	Graham et al.[62]	Lamberton[63]	Lamberton[63]	Radovic[64]	Radovic[64]
	Isotropic Ultasound	Isotropic RUS	Isotropic RUS	Isotropic RUS	Cubic RUS
c_{11}(GPa)	369.24	391	387	393	392.7
c_{44} (GPa)	122.66	129	128	130.9	130.8
c_{12} (GPa)	123.92[a]	132[a]	132[a]	131.2	130.8

[a] $c_{12} = c_{11} - 2c_{44}$.

4.2. High strain rate/high stress mechanical tests

During the last 5 years,[65] the response of AlON under varying dynamic loading conditions has been investigated. These investigations have dealt with: (1) shock wave compression of AlON to determine its equation of state, shear strength sustained under shock wave compression and spall strength,[66–69] (2) onset of damage in AlON under uniaxial stress loading,[70] (3) and under edge-on impact (EOI) using dynamic photoelasticity.[71] Since defects can play a critical role in severe impact events (certainly in quasi-static mechanical stress), it is essential to unambiguously quantify their affect on failure.

4.2.1. Edge-on impact

The interaction of high velocity objects with brittle ceramics results in the formation and propagation of damage and severe fragmentation. An edge-on impact technique, developed at the Fraunhofer-Institut für Kurzzeitdynamik, Ernst-Mach-Institut (EMI), Efringen-Kirchen, Germany, coupled with a Cranz-Schardin high-speed camera, has been successfully utilized to visualize dynamic fracture in AlON during the first 20 μs after impact, characterizing the macroscopic fracture patterns, single crack velocities and crack front velocities (damage velocities) as a function of impact velocity and impactor geometry.[71] Two different optical configurations were employed: a regular transmitted light shadowgraph set-up (Fig. 15) was used to observe wave and damage propagation and a modified configuration, where the AlON specimens were placed between crossed polarizers and the photo-elastic effect was utilized to visualize the stress waves.

Fig. 16, is a shadowgraph of an impact by a steel solid cylinder at 381 meter per second after 8.7 μs showing the influence of preexisting defects on the damage front. Fig. 17 illustrates a sequence of photos at various times using a spherical steel impactor: the top series in plane light and the bottom series with crossed polarizers.[71,72] A comparison of a finite element analysis (FEA) simulation using Abaqus Explicit (Abaqus is a commer-

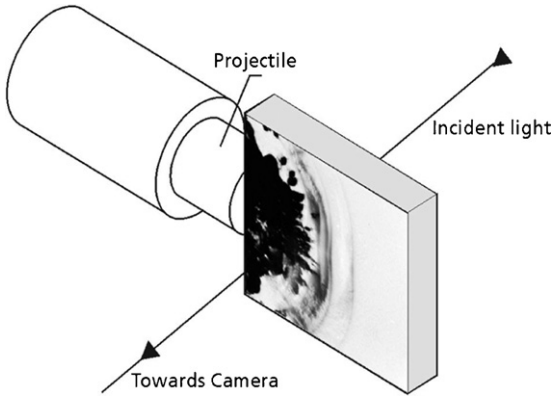

Fig. 15. Edge-on impact test configuration at EMI; AlON sample is 100 mm × 100 mm × 10 mm.[72]

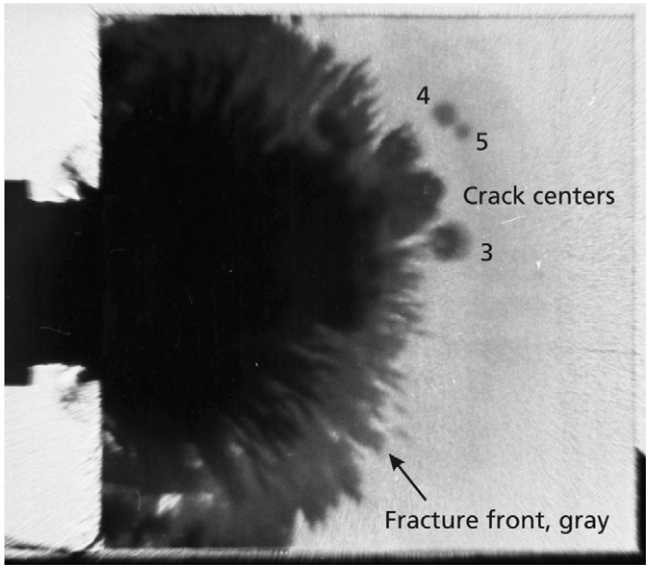

Fig. 16. Edge-on impact shadowgraph 8.7 μs after impact of a steel solid cylinder impactor at a velocity of about 400 m/s.[72]

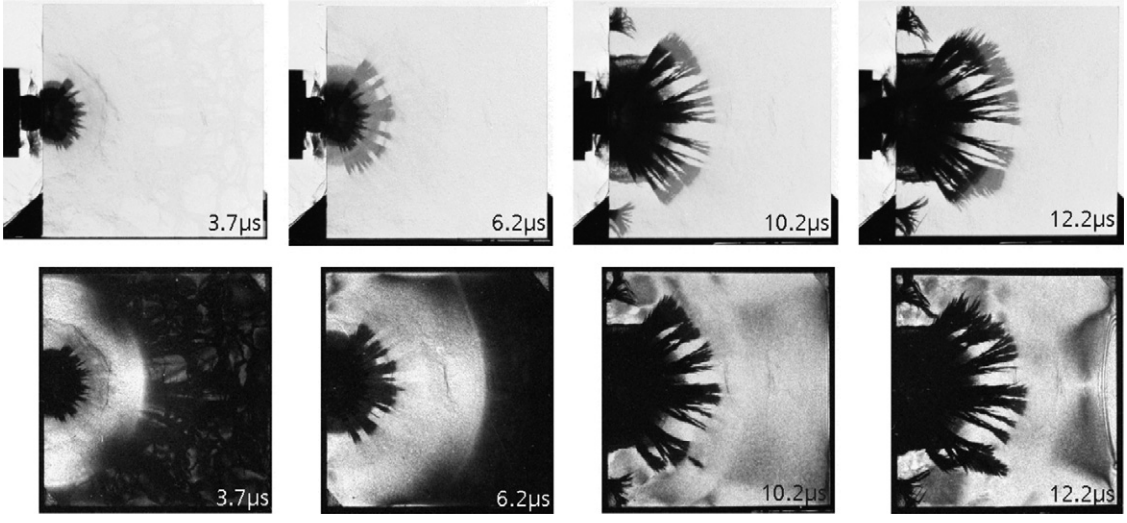

Fig. 17. Edge-on impact photos in plane and crossed polarized light-steel sphere impactor at 429 m/s: top series in plane light, bottom series in crossed polarized light.[72]

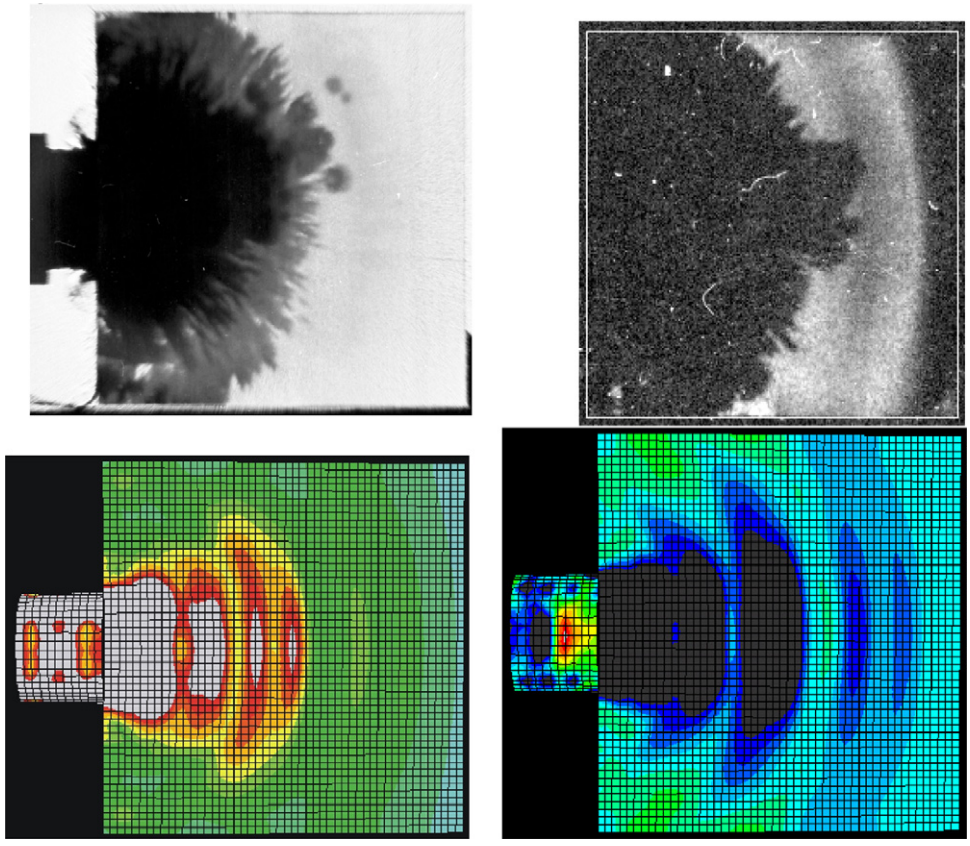

Fig. 18. Comparison of EoI photographs with finite element analysis −8.7 μs with steel cylinder at a velocity of about 400 μs: top left shadow graph (damage), top right in crossed polarizers—stress birefringence, bottom right is the FEA results for the S11 principal stress (compression) and bottom left is the von Mises stress (shear dominated) from the FEA simulation.[72]

cial software package for finite element analysis developed by SIMULIA, a brand of Dassault Systemes S.A.) that was fully 3D,[72] to these EOI results is shown in Fig. 18. It is noteworthy that the main damage front almost exactly corresponds to the von Mises stress (shear intensive) and the main stress wave, however, is parallel to the main compression wave. Finally, additional numerical simulations[73] are being carried out at EMI as shown in Fig. 19. This is a simulation snapshot of an impact comparable to the series in Fig. 17 using a spherical impactor at 0.9 μs. An actual AlON microstructure was used in the simulation. More details can be found in the referenced report. Actual microstructures were used in the simulation and estimates were made of the strength of the grain boundaries. The single crystal elastic constants were not used. The intragranular deformation and failure mechanisms were not included. As can be seen in Fig. 20, [74] it appears that micro-cleavage can occur in the grains themselves; more robust simulations should attempt to include these mechanisms at the grain level.

4.2.2. *Kolsky bar dynamic tests*

High-speed photography has been used[70] to observe the dynamic failure of transparent AlON undergoing uniaxial, high strain rate compression with a modified compression Kolsky bar technique shown in Fig. 21. The high-speed photographs are correlated in time with direct measurements of the stresses in the sample. The dynamic activation, growth and coalescence of cracks and resulting damage zones from spatially separated internal defects was directly observed and correlated to

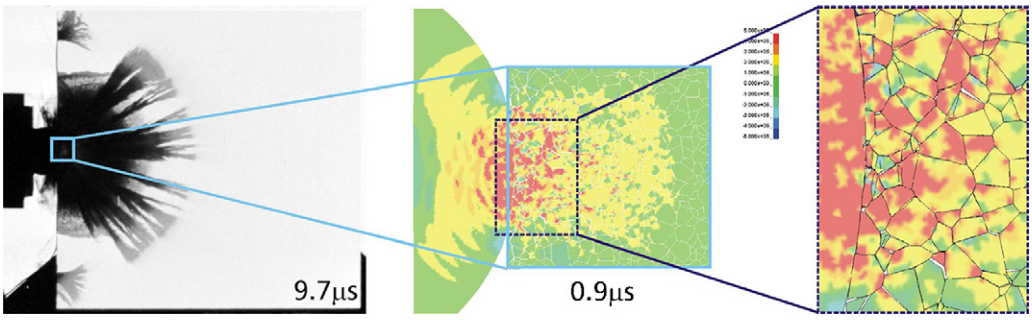

Fig. 19. A simulation snapshot[73] of the series in Fig. 17 of a 7.8 mm × 7.8 mm section of the original 100 mm × 100 mm tile.

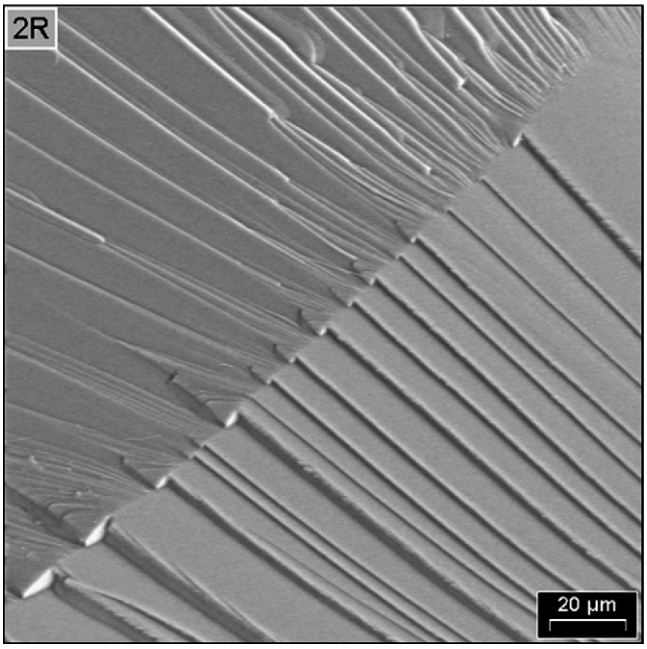

Fig. 20. A fractograph illustrating pronounced cleavage and a twin in an AlON grain that was on the tensile surface of a biaxial flexure test specimen approximately 1 mm away from the fracture initiation site.[74]

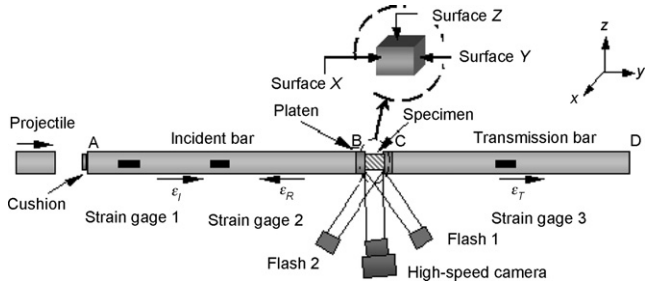

Fig. 21. Schematic drawing of the Johns Hopkins high-speed photography Kolsky bar set-up. Sample size is 5 mm × 4 mm × 2 mm.[70]

the macroscopic loss of load-carrying capacity and ultimate catastrophic failure. It can be easily seen in Fig. 22 that the damage evolution and eventual catastrophic failure initiates at pre-existing defects in the AlON material. Careful examination of the resulting fragments from the tests revealed that the defects were probably carbon-based material that was the result of incomplete reaction during the carbothermal reduction powder synthesis process.

4.2.3. Plate impact studies

Shock wave experiments have been performed on AlON with varying densities, which could reflect either differences in composition or porosity.[66–69] The densities and elastic properties of

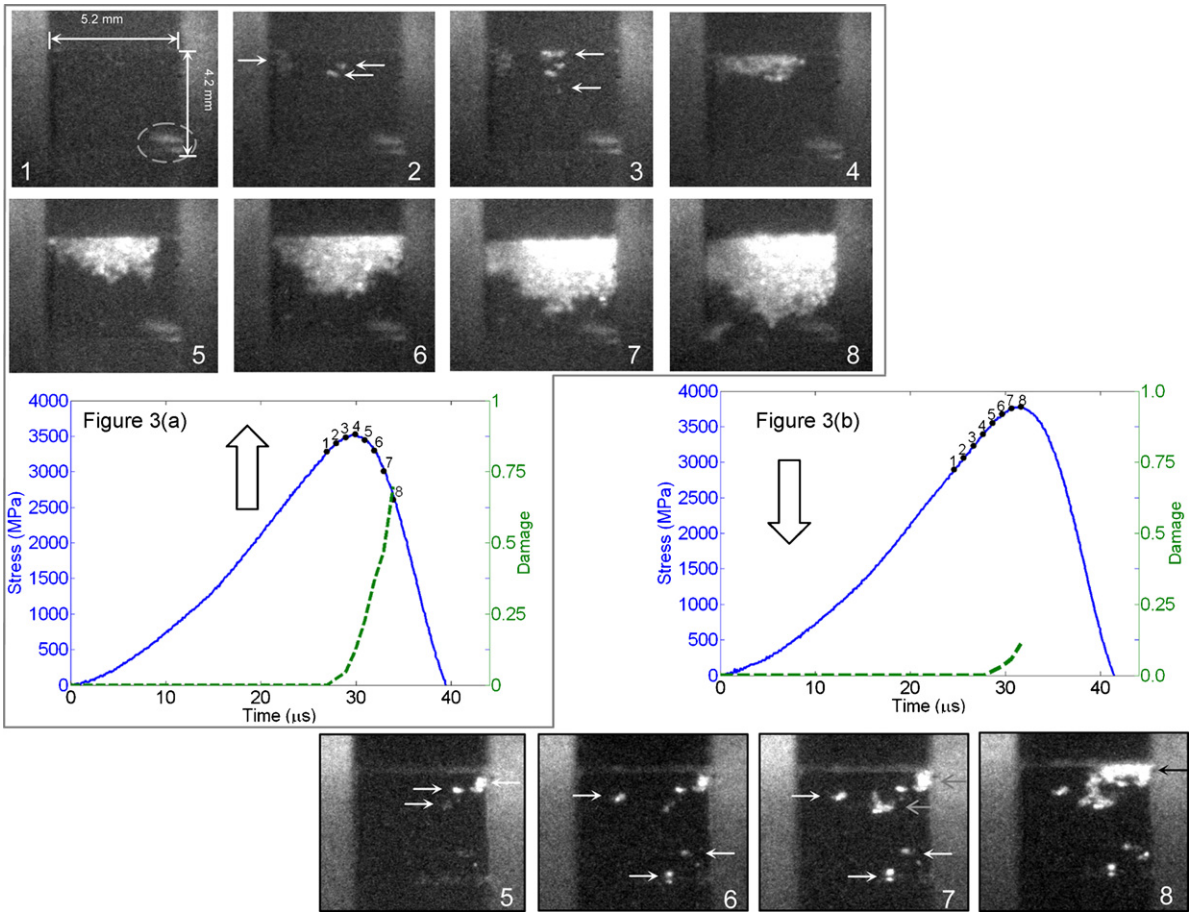

Fig. 22. Kolksy bar photographs and related stress/time curves for two AlON samples.[70]

Table 3
AlON elastic properties from shock wave investigations

Property	Reference[66]	Reference[66]	Reference[67]	Reference[68]	Reference[69]
Ambient					
Density (mg/m^3)	3.51	3.68	3.59	3.67	3.67
Ultrasonic wave velocity (km/s)					
Longitudinal	10.3	10.5	10.27	10.25	10.25
Shear	5.91	5.91	5.91	5.88	5.88
Bulk	7.715	7.980	7.675	7.679	7.679
Elastic modulus (GPa)					
Bulk	208.91	234.34	211.46	215.81	215.81
Shear	122.60	128.54	125.39	126.54	126.54
Poisson's ratio	0.255	0.268	0.252	0.255	0.255
Shock					
HEL (GPa)	10.5	10.9	10.7	11.6 ± 0.6	10.04 ± 0.6
Shock velocity (km/s)			7.67	8.08	7.64
Slope (s)			1.3	0.761	0.779

the materials used in these investigations are given in Table 3.[65] The elastic response of AlON under shock wave propagation, reflected in the Hugoniot elastic limit (HEL), did not indicate any significant deviations from expectations. However, the inelastic response of AlON[66–68] seem to suggest differing patterns and appear to be stress dependent. These issues are currently under study by Dandekar et al. at the Army Research Laboratory.[75] His current analysis indicates that the compression of AlON appears to undergo a shift around 16–20 GPa becoming relatively more compressible. However, AlON continues to retain shear strength at higher stresses. The reason for the observed shift remains to be understood and explained satisfactorily. There are also inconsistencies in some of the shock data reported so far[68,69] that remain to be resolved. In addition, Sekine et al.[68] have deduced from plate impact experiments up to 180 GPa that AlON undergoes a phase transition at about 130 GPa, with the Al shifting from fourfold to sixfold coordination.

$$Al_8^{IV}\,Al_{15}^{VI}\,\square^{VI}\,O_{27}\,N_5 \Longrightarrow Ca^{VI(II)}Ti_2^{VI}O_4\text{ - type structure}$$

5. Commercial products

ALON^{TM} has found many applications over the years including the following: military aircraft and missile domes, transparent armor, IR windows, hyper-hemispherical domes, laser windows, military aircraft lenses, semi-conductor processing applications, and scanner windows (point of sale (POS) windows). Fig. 23 illustrates some of the ALON^{TM} products sold by the Surmet Corporation. There still remain issues associated with the high cost of final machining and finishing.

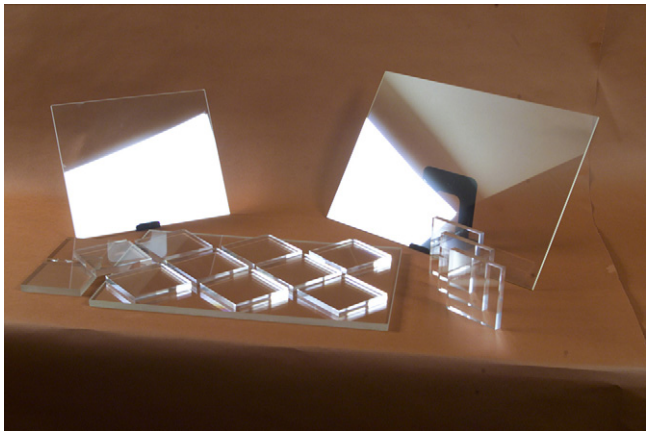

Fig. 23. Commercial ALON^{TM} products; Courtesy: Lee M Goldman, President ALON Products Group, Surmet Corporation, Burlington, Massachusetts, USA.

6. Summary and conclusions

Starting with the first indications of a nitrogen stabilized alumina spinel by Yamaguchi and Yanagida, 1959,[1] and the fabrication of translucent material in 1979,[13] it has taken over 40 years to begin to show more widespread commercial applications. AlON is a unique material exhibiting many important properties which make it useful in many applications and others yet to be determined. Although there has been extensive research on the material, especially more recently because of increased commercial interest, extensive systematic powder synthesis and processing studies have not been carried out to determine alternate, more cost efficient routes to fully dense transparent bodies. Further optimization of reaction sintering and transient liquid phase sintering could be important processing routes. For example, recent work has clearly demonstrated the apparent importance of vapor phases during processing. Refined lattice parameter measurements are a convenient way to determine composition and the shift in composition from starting materials. Commercial availability of appropriate AlON powders produced by a variety of techniques would clearly be important to allow for processing work by various groups. Current AlON material exhibit average grain sizes on the order of 150–200 μm; methods of grain size control, especially at the nano-scale could create materials with improved properties. Because of its high hardness, there are, however, still significant cost issues associated with final machining and polishing, especially for large bodies.

There has been more recent interest in the high strain rate mechanical properties of AlON. Systematic Kolsky bar and edge-on impact work has demonstrated the role of carbonaceous

defects in the failure of AlON and plate impact studies suggest apparent unidentified softening deformation mechanisms at about 15–20 GPa. AlON transparency allows for real time observation during quasi-static and high rate tests and, therefore, is an excellent model material for polycrystalline structural ceramics. In addition, because of its large grain size, the material is more tractable for modeling and computer simulation studies of deformation and failure. However, in order to have more robust analysis, the grain boundary strength and intragranular deformation (e.g. twinning) and failure (cleavage) mechanisms must be identified. The full set of elastic constants ($c_{ij}s$) must be determined unambiguously for higher fidelity modeling.

Acknowledgements

The authors appreciate the critical review of Robert Dowding, James Sands and Costas Fountzoulas.

References

1. Yamaguchi, G. and Yanagida, H., Study on the reductive spinel—a new spinel formula $AlN–Al_2O_3$ instead of the previous one Al_3O_4. *Bull. Chem. Soc. Jpn.*, 1959, **32**, 1264–1265.
2. Long, G. and Foster, L. M., Crystal phases in the system Al_2O_3–AlN. *J. Am. Ceram. Soc.*, 1961, **44**, 255–258.
3. Adams, I., AuCoin, T. R. and Wolff, G. A., Luminescence in the system Al_2O_3–AlN. *J. Electrochem. Soc.*, 1962, **109**(11), 1050–1054.
4. Lejus, A., Formation at high temperature of nonstoichiometric spinels and of derived phases in several oxide systems based on alumina and in the system alumina–aluminum nitride. *Rev. Int. Hautes Temp. Refract.*, 1964, **1**(1), 53–95.
5. Lefebvre, A. L., Giles, J. C. and Collongues, R., Periodic antiphases in a nonstoichiometric spinel ($9Al_2O_3$–AlN) prepared at high temperature. *Mater. Res. Bull.*, 1972, **7**(6), 557–565.
6. Irene, E. A., Silvestri, V. J. and Woolhouse, G. R., Some properties of chemically vapor deposited films of $Al_xO_yN_z$ on silicon. *J. Electron. Mater.*, 1975, **4**, 409–427.
7. Jack, K. H. and Wilson, W. T., Ceramics based on the Si–Al–O–N and related systems. *Nat. Phys. Sci.*, 1972, **238**, 28–29.
8. Oyama, Y., Solid solution in the ternary system Si_3N_4–AlN–Al_2O_3. *Jpn. J. Appl. Phys.*, 1972, **11**, 760–761.
9. McCauley, J. W. and Viechnicki, D. J., Reaction studies in the Si_3N_4–Al_20_3 system. *Am. Ceram. Soc. Bull.*, 1974, **53**(8), 620.
10. McCauley, J. W., Viechnicki, D. J., Corbin, N. D. and Corkum, D. H., Stability of a spinel phase in the Al_2O_3–AlN system. *Ceram. Soc. Bull.*, 1977, **56**(3), 301.
11. McCauley, J. W., Cubic aluminum oxynitride spinel: stabilization and a new model. *Am. Ceram. Soc. Bull.*, 1977, **56**(8), 731.
12. McCauley, J. W., A simple model for aluminum oxynitride spinels. *J. Am. Ceram. Soc.*, 1978, **61**, 372–373.
13. McCauley, J. W. and Corbin, N. D., Phase relations and reaction sintering of transparent cubic aluminum oxynitride spinel (ALON). *J. Am. Ceram. Soc.*, 1979, **62**, 476–479.
14. McCauley, J. W. and Corbin, N. D., Sintered polycrystalline nitrogen stabilized cubic aluminum oxide material. #4,241,000, 1980.
15. Hartnett, T. M., Maguire, E. A., Gentilman, R. L., Corbin, N. D. and McCauley, J. W., Aluminum oxynitride spinel (ALON^{TM})—a new optical and multimode window material. *Ceram. Eng. Sci. Proc.*, 1982, **3**, 67–76.
16. Raytheon patents: #4,481,300 (1984); #4,520,116 (1985); #4,686,070 (1987) #4,720,362 (1988).
17. McCauley, J. W. and Corbin, N. D., High temperature reactions and microstructures in the Al_2O_3–AlN system. In *Progress in Nitrogen Ceramics*, ed. F. L. Riley. Martinus Nijhoff Pub., The Netherlands, 1983, pp. 111–118.
18. McCauley, J. W., Krishnan, K. M., Rai, R. S., Thomas, G., Zangvill, A., Doser, R. W. and Corbin, N. D., Anion controlled microstructures in the Al_2O_3–AlN system. In *Ceramic Microstructures '86*, ed. J. Pask and A. Evans. Plenum Publishing Corp., 1988, pp. 577–590.
19. Corbin, N. D., Aluminum oxynitride spinel: a review. *J. Eur. Ceram. Soc.*, 1989, **5**, 143–154.
20. McCauley, J. W., *Structure and Properties of AlN and AlON Ceramics. Elsevier's Encyclopedia of Materials: Science and Technology*. Elsevier Science Ltd., 2001, pp. 127–132.
21. Sullivan, R. M., A historical view of ALON^{TM}. In *Proceedings of SPIE, Window and Dome Technologies and Materials IX, v5786*, ed. R. W. Tustison, 2005, pp. 23–32.
22. Li, Yawei and Li, Nam, State of the art: a review of aluminum oxynitride spinel. *Naihua Cailiao (Heat Resistant Mater.)*, 2000, **34**(2), 103–111 (in Chinese).
23. Gauckler, L. J. and Petzow, G., In *Representation of Multi-component Silicon Nitride Based Systems, Nitrogen Ceramics*, ed. F. L. Riley. Noordhoff, Leyden, 1977. pp. 41–62.
24. Fukuyama, H., Nakao, W., Susa, M. and Nagata, K., New synthetic method of forming aluminum oxynitride by plasma arc melting. *J. Am. Ceram. Soc.*, 1999, **82**, 1381–1387.
25. Willems, H. X., Hendrix, M. M. R. M., de With, G. and Metselaar, R., Thermodynamics of ALON II: phase relations. *J. Eur. Ceram. Soc.*, 1992, **10**, 327–337.
26. Zernike, J., *Chemical Phase Theory*. Kluwers Pub. Co. Ltd., Deventer, The Netherlands, 1955.
27. Kaufman, L., Calculation of quasi-binary and quasi-ternary oxynitride systems, III. *Calphad*, 1979, **3**, 275–291.
28. Dumitrescu, L. and Sundman, B. A., Thermodynamic reassessment of the Si–Al–O–N system. *J. Eur. Ceram. Soc.*, 1995, **15**, 239–247.
29. Qiu, C. and Metselaar, R., Phase relations in the aluminum carbide–aluminum nitride–aluminum oxide system. *J. Am. Ceram. Soc.*, 1997, **80**, 2013–2020.
30. Tabary, P. and Servant, C., Thermodynamic reassessment of the $AlN–Al_2O_3$ system. *Calphad*, 1998, **22**, 179–201.
31. Willems, H. X., Hendrix, M. M. R. M., Metselaar, R. and de With, G., Thermodynamics of AlON I: stability at lower temperatures. *J. Eur. Ceram. Soc.*, 1992, **10**, 327–337.
32. Nakao, W., Fukuyama, W. and Nagata, K., Gibbs Free energy change of carbothermal nitridation reaction of Al_2O_3 to form AlN and reassessment of thermochemical properties of AlN. *J. Am. Ceram. Soc.*, 2002, **85**(4), 889–896.
33. Nakao, W., Fukuyama, W. and Nagata, K., Thermodynamic stability of γ-aluminum oxynitride. *J. Electrochem. Soc.*, 2003, **150**, J1–J7.
34. Nakao, W. and Fukuyama, W., Gibbs free energy change of carbothermal nitridation reaction of γ-AlON and its thermodynamic stability. *J. Am. Ceram. Soc.*, 2005, **88**(11), 3170–3176.
35. Wang, X., Li, W. and Seetharaman, S., Thermodynamic study and synthesis of γ-aluminum oxynitride. *Scand. J. Met.*, 2002, **31**, 1–6.
36. Kim, Y. W., Park, B. H., Park, H. C., Lee, Y. B., Oh, K. D. and Riley, F., Sintering, microstructure and mechanical properties of AlON–AlN particulate composites. *Br. Ceram. Trans.*, 1998, **97**(3), 97–104.
37. Kim, Y. W., Park, H. C., Lee, Y. B., Oh, K. D. and Stevens, R., Reaction sintering and microstructural development in the system Al_2O_3–AlN. *J. Eur. Ceram. Soc.*, 2001, **21**, 2383–2391.
38. Maghsoudipour, A., Bahrevar, M. A., Heinrich, J. G. and Moztarzadeh, F., Reaction sintering of AlN–AlON composites. *J. Eur. Ceram. Soc.*, 2005, **25**, 1067–1072.
39. Sakai, T., Hot-pressed oxynitrides in the system $AlN–Al_2O_3$, sintering-theory and practice. *Mater. Sci. Monogr.*, 1981, **14**, 591–596.
40. Kollemberg, E. and Ryman-Lipinska, E., Sintern von aluminium-oxinitrid (AlON). *Keramische Zeitschrift*, 1992, **44**(8), 520–524.
41. Wang Xidong, Wang Fuming and Li Wenchao, Synthesis, microstructures and properties of γ-aluminum oxynitride. *Mater. Sci. Eng. A*, 2003, **342**(1/2), 245–250.
42. Rafaniello, W. and Cutler, I., Preparation of sinterable cubic aluminum oxynitride by the carbothermal nitridation of aluminum oxide. *J. Am. Ceram. Soc.*, 1981, **64**(10), C-128.

43. Balasubramanian, S., Sadangi, R. K., Shukula, V., Kear, B. H. and Niesz, D. E., Plasma reaction synthesis of alumina–aluminum oxynitride nanocomposite powders. *Ceram. Trans.*, 2004, **148**, 83–90.
44. Zientara, D., Bucko, M. M. and Lis, J., AlON-based materials prepared by SHS technique. *J. Eur. Ceram. Soc.*, 2007, **27**, 775–779.
45. Turpin-Launay, D., Thevenot, F., Delvoye, F. and Boch, P., Reactive hot-pressing of γ-aluminum oxynitride. In *Ceramic Powders*, ed. P. Vincenzini. Elsevier Sci. Pub. Co., 1983, pp. 891–897.
46. Launay, D., Orange, G., Goeuriot, P., Thevenot, F. and Fantozzi, G., Reaction-sintering of an Al_2O_3–ALON composite determination of mechanical properties. *J. Mater. Sci. Lett.*, 1984, **3**, 890–892.
47. Trabelsi, R., Treheux, D., Goeuriot-Launay, D., Goeuriot, P., Thevenot, F., Orange, G. *et al.*, Friction, wear resistance and mechanical properties of an alumina–γ-aluminum oxynitride composite (ALUMINALON). In *High Tech Ceramics*, ed. P. Vincenzini. Elsevier Sci. Pub., 1987, pp. 2683–2695.
48. Berriche, Y., Vallayer, J., Trabelsi, R. and Treheux, D., Severe wear mechanisms in Al_2O_3–AlON ceramic composites. *J. Eur. Ceram. Soc.*, 2000, **20**, 1311–1318.
49. Li, N., Li, Y. and Wang, J., In *Proceedings of Unified International Technical Conference on Refractories on High Technic Ceramics and Refractories in Si–Al–O–N and Al–O–N Systems*, ed. M. A. Stett, 1997, pp. 1811–1818.
50. Lepkova, D., Yoleva, A., Pavlova, L. and Surnev, B., Insulation AlON ceramics. *Interceram*, 1996, **45**, 87–89.
51. Goursat, P., Billy, M., Goeuriot, P., Labbe, J. C., Villeche-Noux, J. M., Roult, G. *et al.*, Contribution a L'etude du Systeme AL/O/N II: retention D'azote dans les Products D'oxydation de L'oxynitrure D'aluminum γ. *Mater. Chem.*, 1981, **6**, 81–94.
52. Tabary, P. and Servant, C., Crystalline and microstructure of the AlN–Al_2O_3 section in the Al–N–O system I. Polytypes and γ-AlON spinel phase. *J. Appl. Cryst.*, 1999, **32**, 241–252.
53. Fang, C. M., Metselaar, R., Hintzen, H. T. and de With, G., Structure models for γ-aluminum oxynitride from Ab initio calculations. *J. Amer. Ceram. Soc.*, 2001, **84**, 2633–2637.
54. Leffler, Burum, Appel, Carreiro, and McCauley, 1985, U.S. Army Materials Technology Laboratory, unpublished data.
55. Schwarz, M. R., Dr.-Ing. Thesis, High Pressure Synthesis of Novel Hard Materials: Spinel-Si_3N_4 and Derivatives. Darmstadt, 2003.
56. Weiss, J., Greil, P. and Gauckler, L. J., The system Al–Mg–O–N. *J. Amer. Ceram. Soc.*, 1982, **65**(5), C68–C69.
57. Patel, P. Phase equilibrium and kinetics in the multi-component non-oxide Al–O–N system. Ph.D. The Johns Hopkins University, 2000.
58. Patel, P., Gilde, G. and McCauley, J. W., Transient Liquid Phase Reactive Sintering of Aluminum Oxynitride (AlON), #7,045,091, May 16, 2006.
59. Corbin, N. D., The influences of carbon, nitrogen, and argon on aluminum oxynitride spinel formation" M.S., Massachusetts Institute of Technology, 1982.
60. Patel, P., Swab, J. J., Staley, M. and Quinn, G. D., Indentation Size Effect (ISE) of Transparent AlON and $MgAl_2O_4$. Army Research Laboratory, July 2006, ARL-TR-3852.
61. Hartnett, T. M., Warner, C. T., Fisher, D. and Sunne, W., In *Proceedings of the Characterization of ALON™ Optical Ceramic Presented at the Annual Meeting of the American Ceramic Society meeting*, 2005.
62. Graham, E. K., Munly, W. C., McCauley, J. W. and Corbin, N. D., Elastic properties of polycrystalline aluminum oxynitride spinel and their dependence on pressure, temperature and composition. *J. Am. Ceram. Soc.*, 1988, **71**, 807–812.
63. Lamberton, G., University of Mississippi and Hartnett, T. Surmet, personal Communication, August 2005.
64. Radovic, M. and Lara-Curzio, E., Oak Ridge National Lab, personal communication, March 2006.
65. Dandekar, D. P. and McCauley, J. W., Impact induced mechanical response of aluminum oxynitride (AlON), extended abstract. In *Proceedings of the Army Solid Mechanics Symposium*, 2007.
66. Cazamias, J. U., Fiske, P. S. and Bless, S. J., In *Shock Properties of AlON, Fundamental Issues and Applications of Shock-Wave and High Strain Rate Phenomena*, ed. Staudhammer, Murr and Meyers. Elsevier, New York, 2001, p. 173.
67. Vaughn, B. A. M., Proud, W. G. and Field, J. E., Shock Properties of Aluminum Oxynitride, Shock Physics. Cavendish Laboratory Report SP/1092, 2001.
68. Sekine, T., Li, X., Kobayashi, T., Yamashita, Y., Patel, P. and McCauley, Aluminum oxynitride at pressures up to 180 GPa. *J. Appl. Phys.*, 2003, **94**, 4803–4806.
69. Thornhill, T. F., Vogler, T. J., Reinhart, W. D. and Chhabildas, L. C., In *Polycrystalline Aluminum Oxynitride HUGONIOT and Optical Properties. Shock in Compression of Matter*, ed. M. D. Furnish, M. Elert, T. P. Russell and C. T. White. AIP, NY, 2006, p. 143.
70. Paliwal, B., Ramesh, K. T. and McCauley, J. W., Direct observation of the dynamic compressive failure of a transparent polycrystalline ceramic (AlON). *J. Am. Ceram. Soc.*, 2006, **89**(7), 2128–2133.
71. Strassburger, E., Patel, P., McCauley, J. W. and Templeton, D. W., Visualization of wave propagation and impact damage in a polycrystalline transparent ceramic–AlON. In *Proceedings of 22nd International Symposium on Ballistics*, 2005.
72. Strassburger, E., Patel, P., McCauley, P., Kovalchick, C., Ramesh, K. T. and Templeton, D. W., High-speed transmission shadowgrapic and dynamic photoelasticity study of stress wave and impact damage propagation in transparent materials and laminates using the edge-on impact (EOI) method. In *Proceedings of the 25th Army Science Conference*, 2006.
73. Strassburger, E. and Steinhauser, M., Report E 12/07; February 2007, Efringen-Kirchen, Germany Contract No. N62558-05-P-030, Fraunhofer-Institut für Kurzzeitdynamik, Ernst-Mach-Institut (EMI). Efringen-Kirchen, Germany. [Also Army Research laboratory report ARL-CR-605, April 208].
74. Swab, J. J., Gilde, G. A., Patel, P. J., Wereszczak, A. A., McCauley, J. W. and Risner, J. D., Fracture Analysis of Transparent Armor Ceramics, International Conference on Fractography of Glasses and Ceramics IV, Alfred University, July 2000. Eds. J. Varner and G. Quinn, Ceramic Transactions, v. 122. *Am. Ceram. Soc.*, 2001.
75. Dandekar, D. P., Vaughan, B. A. M. and Proud, W. G., Shear strength of aluminum oxynitride. In *Shock Compression of Condensed Matter-2007*, M. Elert, M. D. Furnish, R. Chak, N. Holmes and J. Nghyen. American Institute of Physics, New York, 2008, 978-0-7354-01469-4/07.